



ANNUAL
REVIEWS **Further**

Click [here](#) to view this article's online features:

- Download figures as PPT slides
- Navigate linked references
- Download citations
- Explore related articles
- Search keywords

The Coupled Chemical and Physical Dynamics Model of MALDI

Richard Knochenmuss

Departement für Chemie und Biochemie, Universität Bern, CH-3012 Bern, Switzerland;
email: rknochenmuss@gmx.net

Annu. Rev. Anal. Chem. 2016. 9:365–85

First published online as a Review in Advance on April 6, 2016

The *Annual Review of Analytical Chemistry* is online at anchem.annualreviews.org

This article's doi:
10.1146/annurev-anchem-071015-041750

Copyright © 2016 by Annual Reviews.
All rights reserved

Keywords

coupled physical and chemical dynamics model, MALDI, ionization mechanisms, exciton pooling, ion-molecule reactions

Abstract

The coupled physical and chemical dynamics model of ultraviolet matrix-assisted laser desorption/ionization (MALDI) has reproduced and explained a wide variety of MALDI phenomena. The rationale behind and elements of the model are reviewed, including the photophysics, kinetics, and thermodynamics of primary and secondary reaction steps. Experimental results are compared with model predictions to illustrate the foundations of the model, coupling of ablation and ionization, differences between and commonalities of matrices, secondary charge transfer reactions, ionization in both polarities, fluence and concentration dependencies, and suppression and enhancement effects.

DESCRIPTION OF THE COUPLED PHYSICAL AND CHEMICAL DYNAMICS MODEL

Matrix-assisted laser desorption/ionization (MALDI) (1, 2) was considered surprising and somewhat mysterious when first introduced. The *M* in MALDI was sometimes facetiously interpreted to stand for *magic*. A logical approach when faced with seemingly magical phenomena is to search for correlations between performance and possible contributory factors. The matrix is a key part of the method, so matrix properties such as proton affinity, sublimation temperature, absorption spectra, and functional groups, among others, were examined and compared. No property by itself satisfactorily correlated with MALDI performance. At the same time, it seemed clear that such factors are not completely irrelevant. As a result, the coupled physical and chemical dynamics (CPCD) model was introduced to integrate the various processes believed to be involved in MALDI using ultraviolet (UV) laser excitation.

General reviews of physical and chemical aspects and models of MALDI can be found elsewhere (3, 4). Space limitations allow only for discussion of the CPCD model. In the model (5–7), ionization is separated into primary and secondary processes. Primary processes are those which lead to initial charge separation and involve matrix. Secondary processes constitute the cascade of ion-molecule reactions leading to those ions observed at the detector of the mass spectrometer. Secondary processes also involve analytes, if present. It is not claimed that the CPCD is necessarily a universal model of UV MALDI. Different fundamental mechanisms may be active in different matrices and depend on excitation wavelength. However, to date the model has required only minor modifications for the matrices and analytes to which it has been applied. The model is described and explained. Then it is compared with various data to illustrate aspects of primary and secondary processes, and coupling to ablation.

Primary Ionization Mechanisms

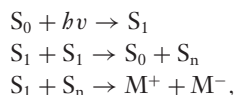
Current debate regarding MALDI mechanisms mostly concerns the initial charge separation step. Models of charge separation may be described as nonthermal, direct thermal, and indirect thermal. The CPCD model is nonthermal. Key processes are, at least transiently, far from equilibrium. Direct thermal models assume that ions are formed by processes that are in thermal equilibrium or close to it. These include, but are not limited to, the polar fluid model (8, 9), which has recently received renewed attention (10, 11). Indirect thermal models require heat (or possibly other energy inputs) not to make ions, but to release ions that are preformed (in some sense) before ablation. The Lucky Survivor model is probably the best-known example (12–14).

The primary mechanism in the CPCD model was initially motivated by a widely used matrix, 2,5-dihydroxybenzoic acid (typically referred to simply as DHB, although there are six isomers). In DHB, fluorescence quenching at high excitation density (15–17) and by traps (18) strongly suggests migration and annihilation (pooling) of excitons. Pooling is a mechanism by which energy is concentrated, and was proposed very early in the development of MALDI (19, 20).

Energy concentration is required because the ionization energy (IE) of DHB is 8.05 eV or 777 kJ/mol (21). In clusters, this falls to approximately 7.8 eV or 750 kJ/mol (22), although the photoionization cross section is very low at the threshold. Typical MALDI lasers generate 337 nm (N₂) or 355 nm (tripled Nd:YAG), corresponding to 3.7 eV (357 kJ/mol) or 3.49 eV (337 kJ/mol), respectively. In both cases, three photons are required to ionize free DHB, DHB clusters, and probably also solid DHB. Direct multiphoton ionization at typical MALDI irradiances is inefficient, but mobile excitons, with pooling, provide a mechanism by which the energy of multiple photons can be stored, transported and concentrated to form ions. This mechanism is consistent with the possibly surprising observation that ion yield depends on fluence (energy deposited,

J/cm²), not irradiance (rate of energy deposition, W/cm²) (23–25). Recently this has been revised (26); it is now clear that the photon number, not fluence, is the key quantity, consistent with a pooling model.

In the CPCD model, the primary ionization process for matrices such as DHB is then:



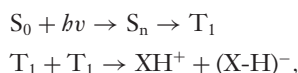
in which S_0 is the ground electronic state, S_1 is the first electronic excited state, and S_n is a higher excited state. The difference between the ionization energy and the final pooled energy is on the order of 1 eV. The electrons emitted with this energy have a mean free path of approximately 10 nm in DHB and other matrices (27, 28), so capture by matrix to form the negative counterion occurs away from the pooling site. This is important, as it limits the rate of recombination and ion loss.

The ionic products may be any that are energetically accessible, but the main possibilities are proton transfer (PT) and electron transfer (ET) ion pairs. The PT pair may be lower in energy than the ET pair for matrices with acidic groups (29), but not for those without (30). Evidence for the ET pair is very direct, in that electron emission from MALDI samples has been observed at fluences well below the ablation threshold (31). Since low energy protons do not have a large mean free path in condensed matter, the PT reaction creates a geminal ion pair that undergoes rapid recombination, with only a few (10^{-6} of those formed) ions escaping (32). Proton transfer is therefore an unlikely or inefficient primary ionization step.

The electron affinity (EA) of DHB is 0.42 eV or 40.5 kJ/mol (33), so the formation energy of the ET ion pair in DHB is $IE - EA = 736$ kJ/mol. Radical matrix cations and anions have been observed in the mass spectra of DHB, but protonated and deprotonated matrices are typically much more abundant. This observation is nevertheless consistent with an ET primary ion pair because conversion to the PT pair is an energetically favorable secondary reaction. The PT pair has a formation energy of 505 kJ/mol (4), or 231 kJ/mol below the ET pair, so the reaction will be efficient.

Numerous matrices proposed for use with analytes of low proton affinity produce only ET matrix ions: radical matrix cations and anions (30). There do not appear to be any matrices that produce only PT matrix ions, even though they may be the lowest in energy. This suggests that in commonly used matrices, the primary ionization process is or includes emission of an electron from a matrix molecule, as assumed in the CPCD model.

In some matrices, such as THAP (2,4,6-trihydroxyacetophenone), intersystem crossing from the singlet manifold to triplet states is efficient because a simultaneous orbital and spin flip transition is symmetry allowed (34). Intersystem crossing is also enhanced in halogenated substances, such as the matrix α -cyano-4-chlorocinnamic acid (ClCCA), and by proximity to halogen-containing species, such as alkali halide salts (external heavy atom effect). Triplets of THAP-related molecules undergo a variety of pooling reactions, including some leading to ionic products (35). In such matrices, the primary process of the CPCD model is taken to be



where X denotes a triplet or a singlet, as either may result. The CPCD model has been extended to include this process.

There is evidence for more complex photodynamics in some matrices, including α -cyano-4-hydroxycinnamic acid (CHCA), sinapinic acid, and ferulic acid, possibly including long-lived metastable species (36–38). The primary step may then need to be further expanded, although the CPCD model was recently successfully used for CHCA (39).

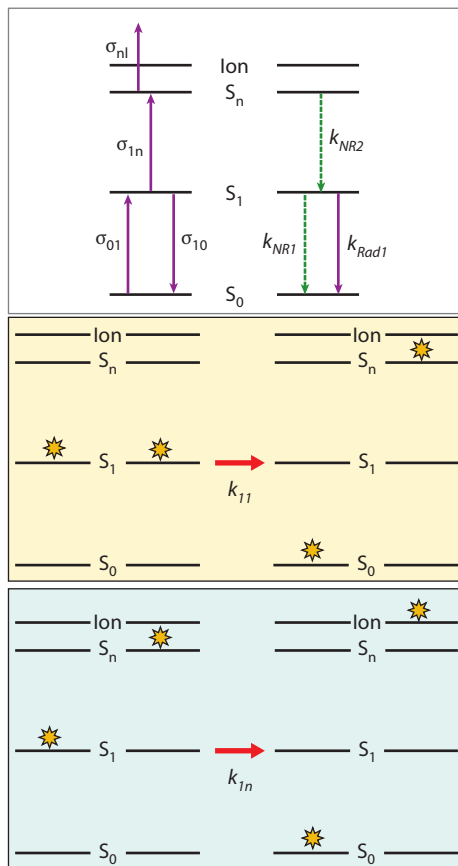


Figure 1

State and transition diagram for primary ionization in the coupled chemical and physical dynamics (CPCD) model. The solid violet arrows represent radiative processes, either absorption or emission, between electronic states of single matrix molecules. The sigmas denote the respective transition cross sections. The dashed lines indicate nonradiative relaxation processes. The two pooling events, which are central to the CPCD, are illustrated in the colored boxes. In both, the total energy of two excited neighboring matrix molecules is redistributed from a delocalized to a localized state. Not shown is hopping of matrix excitons in the crystal lattice.

Figure 1 shows an overview of the radiative and nonradiative steps involved in the CPCD model for primary ionization by singlet pooling. There are a number of parameters, but for simple matrices such as DHB most are available from experiments or by analogy with other materials (5, 6). It is hard to imagine a reasonable model of UV-MALDI that does not include most of these steps; pooling is the only special aspect of this scheme. The $S_1 + S_1$ rate can be determined or inferred from various luminescence experiments (17, 18). The $S_1 + S_n$ rate is more difficult to measure directly. Its main effect is to modulate the total ion yield. Fortunately, relative intensities are largely unaffected over a wide range of $S_1 + S_n$ rates. Such experiments are also the easiest to perform and far more numerous, so uncertainties regarding $S_1 + S_n$ rates have not hindered testing of many aspects of the CPCD model.

The CPCD model exists in two forms. The first is a set of coupled differential rate equations (5–7). For each species in **Figure 1** there is a term corresponding to the arrows connecting it to

the others. The second-order terms, such as pooling, cation/anion recombination, and secondary reactions, are dependent on density and temperature. This important fact couples ion formation and survival to the ablation event and is the basis for the CPCD model name.

In the rate equation approach, ablation is taken to occur upon reaching a specified temperature. The sample changes to a dense gas and expands from the irradiated area of the sample, which acts as a virtual orifice. The velocity, temperature, and pressure after vaporization are given by isentropic expansion equations (40). A key parameter is the C_p/C_v ratio. For polyatomic MALDI matrix molecules this ratio is near 1, so expansion cooling is considerably less than it is in traditional molecular beams using monatomic carrier gases.

Matrix absorption cross sections at typical MALDI wavelengths range from 10^{-18} to 10^{-17} cm², and the 1/e depth is on the order of 300 nm. A CPCD calculation proceeds by layers. A layer nearer the surface reaches a higher temperature and ablates earlier than a deeper layer does because it experiences a higher laser intensity. Because it is hotter, an upper layer also reaches a higher axial velocity. As a result, there is negligible mixing or energy exchange between layers. The layer results are summed, weighted by the mass of each layer. The ablation model of the rate equation approach appears to reproduce several MALDI phenomena, as described below. However, the inherent assumptions are significant.

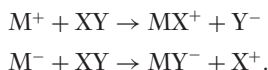
The second form of the CPCD model (41) is based on molecular dynamics (MD) to eliminate assumptions about ablation. Different layers of the sample may vaporize in different ways, and some ejected material may not vaporize at all (42). The breathing sphere framework of Zhigilei et al. (43) was adopted for the MD-based CPCD model. For efficiency, the smallest entity is a molecule, not an atom. Molecules have one vibrational degree of freedom (the breathing mode), which allows interchange of intermolecular kinetic energy and molecular internal energy. The original breathing sphere model does not include the electronic degrees of freedom necessary for the CPCD model; these were added by the author.

In MD simulations, the parameters are probabilities per time step rather than rates. In a sufficiently large ensemble, these give the same results, but in MD simulations the possible occurrence of each kind of event is evaluated at each time step for each molecule. With time steps of a few femtoseconds, hundreds of thousands of molecules, and simulated timescales of several nanoseconds, the method is slow, but essential to refining understanding of ablation-related MALDI phenomena.

Secondary Charge Transfer Mechanisms

After the first ions are created, the material is still dense, so ion–molecule reactions can be extensive. The system tends toward local thermal equilibrium (LTE), but LTE is not reached in MALDI. MALDI spectra often show direct evidence of this. In positive ion mode, matrix radical cations and protonated, sodiated, and potassiated matrix often are observed simultaneously with roughly comparable intensity. The relative formation energies of these ions span hundreds of kJ/mol, so LTE predicts far larger differences in relative intensities than observed.

Secondary reactions of matrix ions may involve adduct formation:



An important special case is the conversion of ET ions to a PT pair (or the inverse):



The energies of these pairs may differ substantially, as for DHB, or only moderately for other species. If XY is a salt, such as an alkali halide, ions such as the commonly observed sodium or

potassium adducts with matrix are formed. In negative ion mode, anion adducts are also observed, though halide adducts are rare due to the low matrix affinities for them.

Direct ionization of analytes (or preformed analyte ions) is not included in the CPCD model. This is not to imply that the pathway cannot exist. For example, some matrix–analyte complexes may be two-photon ionizable (44, 45). Some authors also have suggested that preformed and CPCD-like mechanisms coexist (13). But matrix is normally so much more abundant than analyte (typically at least a factor of 1000), and it is so highly energized by the laser, that matrix ionization is expected to dominate (46).

Secondary reactions include charge transfer between matrix and analyte in both polarities, and between analytes. These reactions are assumed to be reversible. If the dominant matrix ions are PT pairs (reaction products of ET primary ions), secondary reactions with analyte are predominantly PT reactions. Many biologically important analyte classes are most easily observed in protonated or deprotonated form. To estimate PT reaction rates for a wide range of analytes, the CPCD model uses activation energies derived from reaction free energies (47). In the case of ET secondary reactions, a similar free energy relationship may be used, but a different one may sometimes be more appropriate, as found for recombination.

Loss Mechanisms

In addition to primary ionization and secondary charge transfer reactions, recombination of ions to neutrals must be included. As noted above, geminal primary PT pairs suffer high loss rates immediately after formation because the proton cannot diffuse away quickly. MD simulations show that nongeminal recombination is slow until the material melts and ions become mobile (41). At melting, a surge of recombination liberates a considerable amount of heat. This heat pulse accelerates the ablating material, which paradoxically reduces recombination in the plume by accelerating the expansion.

Ion recombination is very exothermic, but therefore also possibly rate limited. For radical ion pairs, and possibly for PT pairs, the initial recombination step is ET. In the case of PT pairs, ET may occur before PT because the range of ET is greater. ET charge neutralization is then followed by hydrogen atom transfer to complete the reaction. Highly exothermic ET is in many cases slower than the collisional rate limit, due to reorganization energy. This is known as Marcus inverted behavior. During the dense period of the MALDI event, when recombination is most extensive, even a moderately reduced recombination rate can result in significantly more ions reaching the detector (48, 49).

RESULTS AND EXAMPLES

The CPCD model is fundamentally simple. It includes laser excitation, ion formation, ion–molecule and ion–ion reactions, and coupling to ablation. These are elements of MALDI that clearly cannot be neglected. The remainder of this review compares model results with experiment.

General Example: Yield Versus Wavelength and Fluence

A significant test of the CPCD model was provided by the two-dimensional dataset of Soltwisch et al. (26). They measured matrix and analyte ion yields versus wavelength and fluence for several matrices including DHB, CHCA, and CICA.

As shown in **Figure 2** and described by Knochenmuss (39), the CPCD model reproduces the CHCA data well. (Results for DHB and CLCCA matrices are shown in **Supplemental Figures 1** and **2**. Follow the **Supplemental Material link** from the Annual Reviews home page at <http://www.annualreviews.org>). In CHCA, analyte yields are highest at wavelengths that are

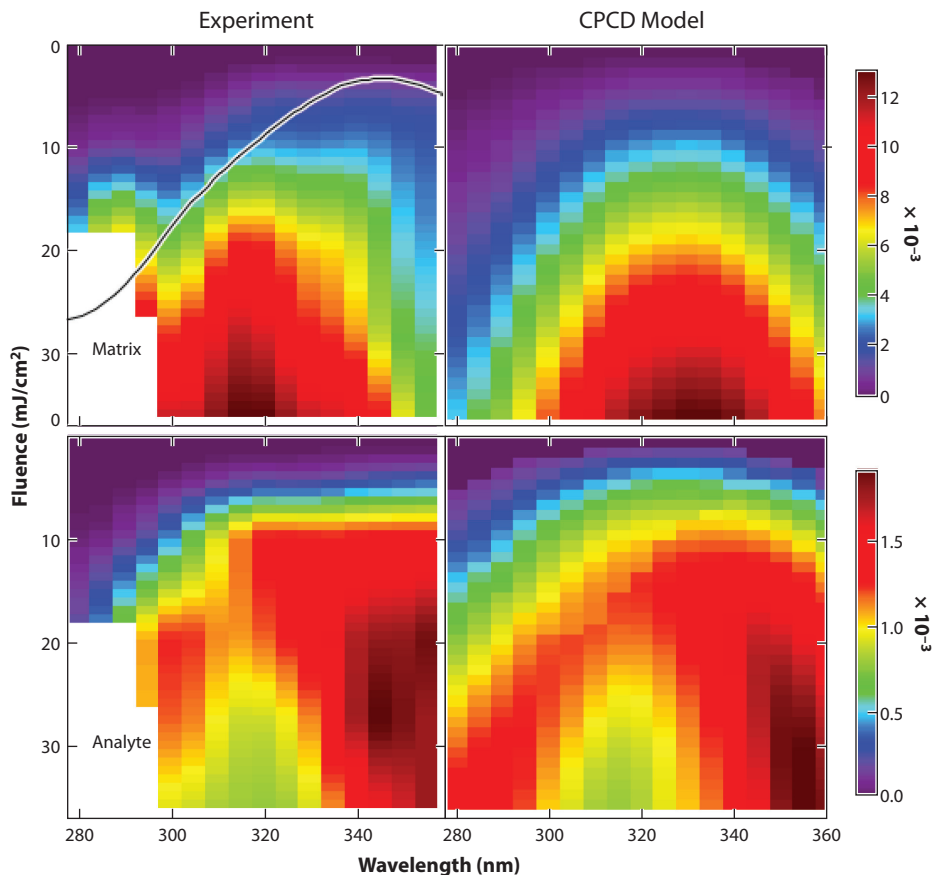


Figure 2

Matrix and analyte MALDI ion yields versus laser wavelength and fluence for CHCA matrix. The left panels show the data reported by Soltwisch et al. (26); the right ones show the corresponding CPCD model predictions. The trace in the top left panel shows the solid-state absorption spectrum (39). Abbreviations: CHCA, α -cyano-4-hydroxycinnamic acid; CPCD, coupled chemical and physical dynamics model; MALDI, matrix-assisted laser desorption/ionization.

the least efficient for matrix, whereas the region where matrix signals are highest corresponds to a dramatic dip in the analyte yield. Neither matrix nor analyte yields correspond straightforwardly with the solid-state absorption spectrum nor with the predicted temperature distribution.

These results illustrate several aspects of UV MALDI that are reflected in the CPCD model. The major differences in matrix and analyte patterns show that they are ionized by separate mechanisms. Maximum matrix yield is found near 315 nm and at maximum fluence. Here, ablation is fastest due to strong absorption and the large excess energy of each photon above the S_1 vibrationless level. Analyte yield is reduced in this region because secondary reactions are kinetically limited by the fast expansion of the plume. Higher analyte yield is found at long wavelengths despite lower matrix yield, partly because more photons are required to reach the same fluence. Because primary ionization is dependent on exciton density, photon number rather than fluence or irradiance is the key parameter. This example shows how the various aspects of MALDI are intertwined and the necessity of including them together in a single model.

Results Relating to Primary Ionization

The varied phenomena illuminate or are a consequence of primary ionization mechanisms.

Evidence for pooling. Evidence for pooling in MALDI matrices has been found in optical emission experiments. If fluorescence in the solid state is moderately efficient, and if pooling affects the fluorescent state, it may be detected by increased quenching at high excitation densities. This has been observed in a number of matrices. See **Supplemental Figure 3** for an example.

Other tools include time- and wavelength-resolved emission (36, 38), pump-probe, and trapping experiments. These show that CHCA, sinapinic acid, and ferulic acid photophysics include more than one active excited state and possibly metastable photochemical products.

Trapping by fluorescent dyes doped into matrix materials provides evidence for exciton hopping and pooling, and also allows confirmation by mass spectrometry. As seen in **Figure 3**, even at a mole ratio of 5×10^{-9} in DHB, sensitized fluorescence of the laser dye DCM [4-(dicyanomethylene)-2-methyl-6-(4-dimethylaminostyryl)-4*H*-pyran] is easily observed (18). At a mole ratio of 4×10^{-6} ,

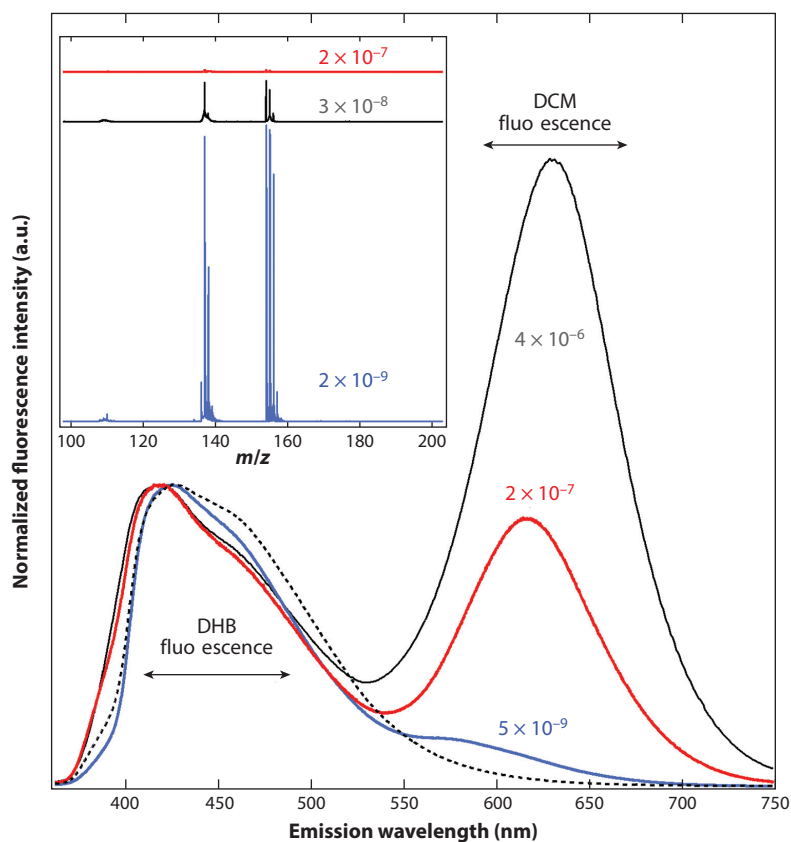


Figure 3

Luminescence spectra of DHB crystals doped with DCM. The spectra have been normalized to the DHB fluorescence maximum. The dashed line corresponds to an undoped DHB crystal. The solid traces are labeled with the mole ratios of DCM to DHB in the crystals. The inset shows the corresponding effect on the MALDI ion yield. Adapted with permission from Reference 18. Abbreviations: DCM, 4-(dicyanomethylene)-2-methyl-6-(4-dimethylaminostyryl)-4*H*-pyran; DHB, 2,5-dihydroxybenzoic acid; MALDI, matrix-assisted laser desorption/ionization.

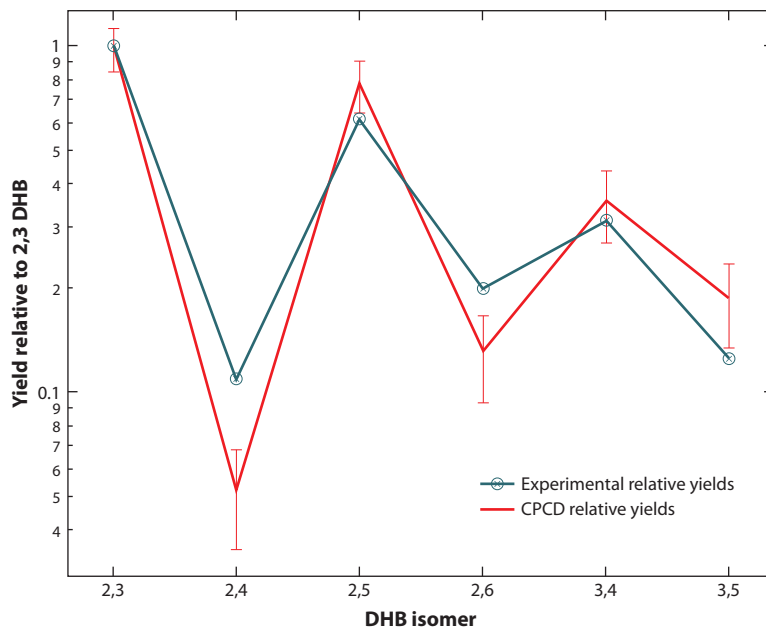


Figure 4

Comparison of experimental and CPCD relative total MALDI ion yields for all DHB isomers. The CPCD error bars reflect the uncertainties in the pooling rate constants estimated from luminescence decay experiments. The experimental values are the average of two sets of measurements. Adapted from Reference 51. Abbreviations: CPCD, coupled chemical and physical dynamics model; DHB, dihydroxybenzoic acid; MALDI, matrix-assisted laser desorption/ionization.

its fluorescence is stronger than that of the DHB host. These results and others can be quantitatively explained by exciton hopping and trapping in the DHB crystal.

The MALDI relevance of exciton trapping is evident in the mass spectra of the doped crystals. Already at 3×10^{-8} mole ratio, the ionization efficiency was strongly reduced (18). Jaskolla & Karas (50) have reported similar results for CHCA matrix.

Isomeric matrices. Pooling is mediated by intermolecular interactions. Kirmess et al. (51) proposed that the same interactions may lead to quenching if only one, rather than both, of the interacting molecules is excited. Then relative pooling rates are inversely proportional to the quenching rates at low excitation density. With this hypothesis, the CPCD model reproduced the relative MALDI yields of the six DHB isomers (**Figure 4**).

Extrapolation from the well-studied 2,5-DHB isomer to the other isomers required only the solid-state absorption spectra and the luminescence decay curves. The wide variation in DHB isomer MALDI performance has long been a puzzle. Attempts to find a correlation with various properties, such as proton affinities or sublimation temperatures, were not successful. A thermal model was also compared to the data, and was found to deviate by many orders of magnitude, in a manner uncorrelated with the pattern found in **Figure 4** (51).

Absolute ion yield and yield versus fluence. The DHB isomer comparison used relative ion yields, as few measurements of absolute yields exist. The absolute yield is strongly dependent on

the second pooling step, which is difficult to measure or estimate. Fortunately, it has little effect on relative comparisons, enabling tests of the CPCD model.

The $S_1 + S_n$ pooling rate in 2,5-DHB was originally set to reproduce available yield data, in the 1×10^{-4} range, and to fit time-delayed pump-probe experiments. Primary ion yield peaked at a delay of approximately 2 ns (5, 52). The CPCD model predicts the delayed peak as a consequence of the kinetics of ion formation, loss, and plume expansion (see **Supplemental Figure 4**). Electron emission versus fluence from MALDI samples was also found to follow the CPCD pooling prediction, as discussed below. Evidence was later reported for lower absolute yields in the 10^{-6} to 10^{-8} range (10, 11). Such experiments are difficult, and the results are therefore open to question, but were used to argue that the CPCD model must be incorrect (10, 53–55). However, simply reducing the $S_1 + S_n$ pooling rate constants gives excellent agreement with the data for DHB and CHCA matrices (**Supplemental Figure 5**) (56). The alternative thermal model did not provide a good fit.

Crystal morphology and MALDI sample variability. The variability of MALDI mass spectra and their dependence on sample preparation methods are two significant drawbacks of the technique, for reasons not fully understood. The inhomogeneous distribution of the analyte in the matrix can play a significant role (57), but even pure matrix can be highly variable.

The CPCD model provides a simple explanation based on the mobility of excitons and on pooling. Both are a consequence of intermolecular interactions, which are in turn dependent on molecular packing in the solid. Packing is also reflected in macroscopic morphology. Differently prepared samples, or even crystals within one sample may exhibit different morphology, which has been correlated with MALDI performance (58).

Morphologically different THAP crystals are an example (**Supplemental Figure 6**) (59). Fluorescence, intersystem crossing, and phosphorescence rates vary in samples prepared from different solvents. Triplet-related properties were found to correlate with MALDI performance (59), consistent with the pooling aspect of the CPCD model.

Two-photon ionization of matrix-analyte complexes. A wide variety of analytes are amenable to MALDI analysis, suggesting that analytes are mostly inert with respect to primary ion formation. This is not always true; for example, DHB interacts strongly with proline in 1:2 or 1:4 complexes. Their ionization potentials (IP) are reduced to within the two-photon range (44, 60–62).

If analyte is present in high concentration (several percent), ionization of matrix-analyte complexes can be a non-negligible contributor. However, high concentrations are normally avoided because of suppression effects. At typical concentrations, matrix pooling remains the dominant pathway (**Supplemental Figure 7**) (46). This is significant, because analyte type has not been found to correlate with total ion yield. The CPCD model is thus consistent with experimental data, in that ionization is overwhelmingly a matrix-related phenomenon.

Primary ionization and the supporting surface. MALDI ion production tends to decrease as a function of laser shots on a single spot (63). But if ablation continues down to the supporting substrate, a significant increase in ion production can be observed in many cases. By comparing thick and thin samples on different metals, Knochenmuss and colleagues (63, 64) proposed that this increase is a consequence of matrix excited states interacting with the metal. Ionization with two photons becomes possible in a sequential two-step process.

The CPCD model is easily modified to handle this. The initial $S_1 + S_1$ pooling step leads directly to ions, and the subsequent $S_1 + S_n$ step is omitted. A mixed calculation is also possible

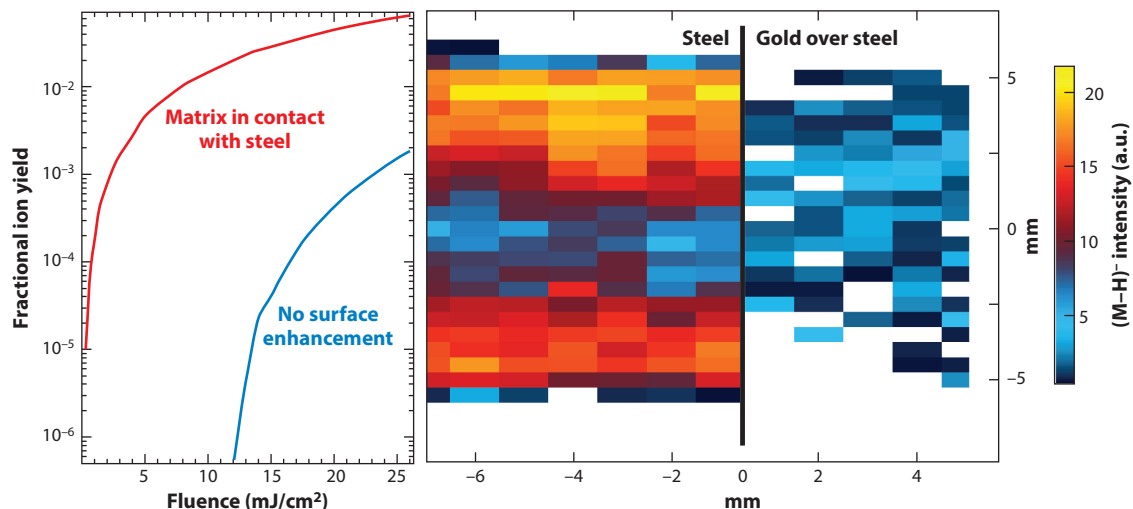


Figure 5

(Left) The enhancement on steel is consistent with the excited-state ionization mechanism of the CPCD model, modified to account for the interaction with the metal conduction band. See also References 63 and 64. Abbreviations: CPCD, coupled chemical and physical dynamics model; MALDI, matrix-assisted laser desorption/ionization. (Right) MALDI image of a sprayed track of sinapinic acid, $(M-H)^-$ ion. The track was approximately 1 cm wide and crossed the boundary between the steel substrate and a region where the steel was coated with 40 nm of gold. The enhancement is largest on the thinner upper and lower edges of the track.

by combining the two models as a function of sample thickness. The modified model predicts enhancements in ion yield of two or more orders of magnitude, as observed (63, 64).

Also very well predicted is electron emission versus fluence of thin samples, the form of which verifies the sequential two-photon nature of the process (**Supplemental Figure 8**). This effect depends on the metal and matrix. For matrices with a high-lying LUMO, the work function of the metal must be low for enhancement. This is reflected in MALDI images of sinapinic acid across a steel-gold interface (**Figure 5**). Neither the thermal nor the optical properties of the substrate explain the effect (63, 64).

[▶ Supplemental Material](#)

Results Relating to Ablation

Because it modulates ionization processes, ablation is an important part of MALDI and of the CPCD model.

Plume characteristics. The MD-based CPCD model has provided insight into ablation/ionization coupling (65). Although “desorption” appears in the name, MALDI is generally a violent ablation with various subregimes. The energized matrix may initially be either stress or thermally confined. Surface layers generally vaporize completely, but phase explosion or rapid expansion in less-energized lower layers causes ejection of chunks of condensed material that only partially vaporize downstream. These chunks have been observed (42), and are central to models that require clusters (12–14, 66–68). However, MD simulations suggest that few analyte ions are released from such clusters. Short or intense laser pulses may also lead to spallation of large, cold chunks. Plume temperatures, pressures, and velocities vary strongly and systematically with depth from the original surface. Models that assume these are constant are clearly oversimplified. See **Supplemental Video 1** for an example of a MALDI MD simulation.

First emission of electrons and ions. Electrons have been observed from MALDI matrices at fluences well below the ion emission threshold (31). This phenomenon arises naturally in the MD-based CPCD model, as a consequence of the electron capture cross section (27, 28). Electrons from primary ionization can escape from the top sample layer, which thereby becomes positively charged. Matrix ions are then ejected by electrostatic repulsion, even before melting begins. This finding is consistent with the data of Bökelmann et al. (69), who found two populations of matrix ions: early and fast and later but slower (see **Supplemental Figure 9**).

In the MD-based CPCD model, analytes that are significantly larger than the matrix are not emitted early, unlike matrix ions. The ratio of electrostatic forces to cohesive energy is lower for analytes, so they remain in the condensed phase until it disintegrates (65). This too is consistent with the Bökelmann data, which show analyte ions appearing later and with lower velocities than the early matrix ions.

Spot size. MALDI yield depends on the laser focus at constant fluence (70–73). More ions are generated by larger spots, but the fractional yield is lower (ions/neutrals). The effect is particularly evident for small spots.

In the CPCD model, the plume is a molecular beam emitted from the irradiated spot. It may be a nearly ideal beam because the ablated layer is only a few hundred nanometers thick, while the diameter is usually greater than 100 μm . Expansion is determined by the ratio of diameter to downstream distance. The plume density at a given distance is thus modified by spot diameter. Bimolecular reactions such as pooling and neutralization depend on the plume density. MALDI ion yield is thus also a function of spot diameter. The dependence is predicted to be nonlinear, as observed (**Supplemental Figure 10**). Also in agreement with experiment are ion yields versus fluence, for different spot sizes (72).

Initial sample temperature. The temperature of the sample before irradiation is rarely controlled but is relevant for MALDI performance (74). As demonstrated with DHB over a range of 150°C, total yield does not change monotonically but exhibits a broad maximum (75). The CPCD model reproduces this effect (**Supplemental Figure 11**). It is another manifestation of the interaction between plume expansion and bimolecular reaction kinetics. Heating the sample initially increases ion yield because recombination losses are lower if the plume expands slightly faster. At high initial temperature, ablation begins too early, cutting off primary ion formation. In a thermal model, ion yield must increase monotonically, because the peak temperature increases with the starting temperature.

MALDI from restricted volumes. In conventional MALDI, the plume can freely expand, but variants use structured substrates such as high-aspect-ratio silicon pillars (76–78). The plume emitted from the capillary volume between such pillars is initially subject to radial confinement. This directs and axially accelerates the plume, changing the density-versus-time and distance profiles. Perhaps counterintuitively, the overall effect is to hasten approach to the collision-free regime. The CPCD model predicts this is favorable for matrix yield but not for analyte ion yield (79). Matrix yield is affected by recombination losses, which decrease in capillary ablation. Analyte ion yields depend on secondary reactions, which benefit from increased matrix ion concentration, but the simultaneous reduction in secondary rates is a larger effect, causing a net drop in analyte ion yield (**Supplemental Figure 12**). The utility of MALDI from structured substrates will therefore mostly depend on improvements unrelated to secondary plume reactions. This may include substrate-enhanced ionization, or better laser absorption, using structures as antennae (76).

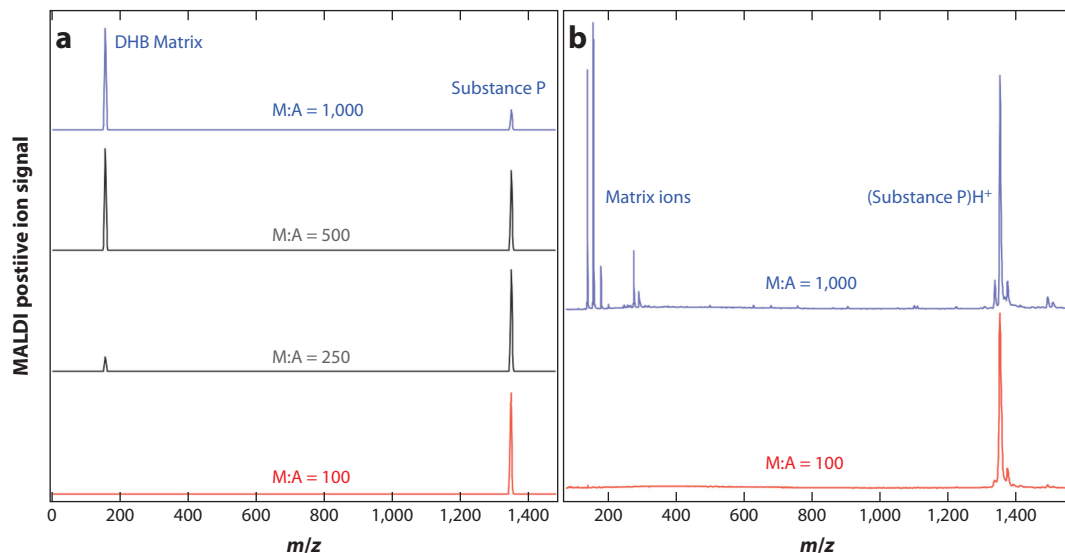


Figure 6

Positive ion MALDI spectra of substance P in DHB matrix at two different molar mixing ratios. If sufficient analyte is present, as in the lowest traces, all matrix ions can be suppressed, including protonated matrix, other cation adducts, and photochemical products (80). Panel (a) shows the corresponding CPCD predictions at 20 mJ/cm² and secondary reaction energy -150 kJ/mol; panel (b) shows experimental data. Note that all matrix ions should be summed for comparison to predictions from the model. Abbreviations: CPCD, coupled chemical and physical dynamics model; DHB, dihydroxybenzoic acid; M:A, matrix:analyte molar ratio; MALDI, matrix-assisted laser desorption/ionization.

Results Relating to Secondary Reactions

The most analytically important aspects of the CPCD model are those involving secondary reactions, because they generate analyte ions.

Matrix suppression effect. An interesting MALDI phenomenon is the disappearance of matrix ions at higher analyte concentration in the sample (80, 81). In **Figure 6**, at a matrix:analyte molar ratio of 1,000:1 both protonated peptide substance P and a variety of DHB matrix ions are prominent in the mass spectrum. If more substance P is added, to a ratio of 100:1, no matrix ions are observed. A similar effect can be observed for negative ions (81). This is the matrix suppression effect (MSE). MSE is believed to be very general, and has been observed with a variety of different matrices and analytes (82). It is associated not only with PT secondary reactions, but also with ET and reactions to form other ion adducts (30).

In addition to analyte concentration, laser fluence is the major experimental parameter that affects MSE. At a given analyte concentration, MSE may be observed at low fluences, but a matrix signal can reappear if the fluence is sufficiently increased. Similarly, at higher fluences, more analyte is required to induce MSE.

The molecular weight of the analyte also plays a role in MSE. Higher-molecular-weight analytes are effective at lower matrix:analyte ratios (81) (**Supplemental Figure 13**). MSE is also correlated with the thermodynamics of secondary charge transfer reactions. MSE requires at least one favorable reaction and occurs more readily if the reaction free energy is more favorable (**Supplemental Figure 14**).

[▶ Supplemental Material](#)

All characteristics of the MSE are predicted by the CPCD model. The most important is simply the existence of the effect. MSE results from depletion of matrix primary ions by secondary reactions with analyte. The existence of the MSE implies that the model of separate primary and secondary steps is correct, and that primary ion yields and secondary reaction rates are in the correct ranges. Both the analyte concentration and fluence dependencies reflect the relative amounts of primary ions and secondary neutrals. At low fluence there are fewer of the former, and at high analyte concentration there are more of the latter. The kinetics of bimolecular secondary reactions leads to the observed behavior. The analyte molecular weight effect appears because secondary charge transfer rates in the expanding plume depend on the collision cross sections of the matrix-analyte pair. In MALDI the molecular weight range of analytes is large, so this effect is readily apparent (**Supplemental Figure 13**).

In the CPCD model, the conditions for MSE (analyte concentration, fluence) are correlated with the exoergicity of the forward secondary reaction via the reaction rate. A more negative ΔG value implies a lower activation energy and a faster forward reaction. This is likely to be widely valid for adduct (e.g., H^+ , Na^+) transfer reactions but may not always apply to ET secondary reactions, as noted by Knochenmuss & Zhigilei (48). The reaction rate effect is most apparent at small ΔG values, as illustrated in **Supplemental Figure 14**.

MSE can occur even when analyte and matrix are observed as different types of ions, such as proton and alkali metal adducts. This implies that the corresponding ions can interconvert in the plume. Interconversion of free ions and neutrals is energetically accessible at MALDI temperatures (83), but most interconversions undoubtedly take place in the early dense period, where solvation modulates the energetics somewhat.

Analyte suppression effect. Secondary reactions are not limited to matrix and analyte. They also occur between analytes, as shown in **Figure 7** for an equimolar mix of five analytes undergoing ET secondary reactions (30, 83).

As for MSE, concentrations, relative concentrations, and reaction energetics are key factors for ASE. As demonstrated in **Figure 7**, the relative intensities of the analytes are never completely correct, and they become less representative of the original sample composition as the matrix:analyte molar ratio decreases. In this example, ASE is correlated with the IP value. The species with the highest IP value (7.06 eV) is suppressed most, whereas the species with the lowest IP value (6.04 eV) is always observed. Although it is tempting to invoke direct charge exchange between analytes, this rarely, if ever, reflects the true mechanism of ASE.

In addition to ASE, MSE is seen in **Figure 7**, and it becomes strong before ASE is fully developed. ASE is always accompanied and preceded by MSE because analyte concentrations in normal sample preparations are too low for direct analyte-analyte reactions to play a significant role. Instead, analytes are indirectly coupled by reactions with matrix.

Although coupling could occur via the reverse of secondary reactions (which are included in the CPCD model), this usually plays a small role. For most analytes and common matrices, secondary reactions are sufficiently favorable that the reverse reactions are too slow to allow extensive charge exchange on the MALDI timescale. Instead, the kinetics of the forward reactions are limiting. If analyte A reacts faster with M^+ than analyte B does, and concentrations are high enough for MSE, then formation of analyte B^+ is limited because analyte A depletes available M^+ . Further evidence that the reactions include intermediate steps is that ASE, like MSE, occurs between ions of different types. See **Supplemental Figure 15** for an example. CPCD predictions for analyte reaction kinetics also were validated by time-resolved data (**Supplemental Figure 16**).

The effect of a forward kinetic limit may be similar but not identical to reversible exchange. Forward rates are correlated with reaction free energy but not identically so. Analytes D and C

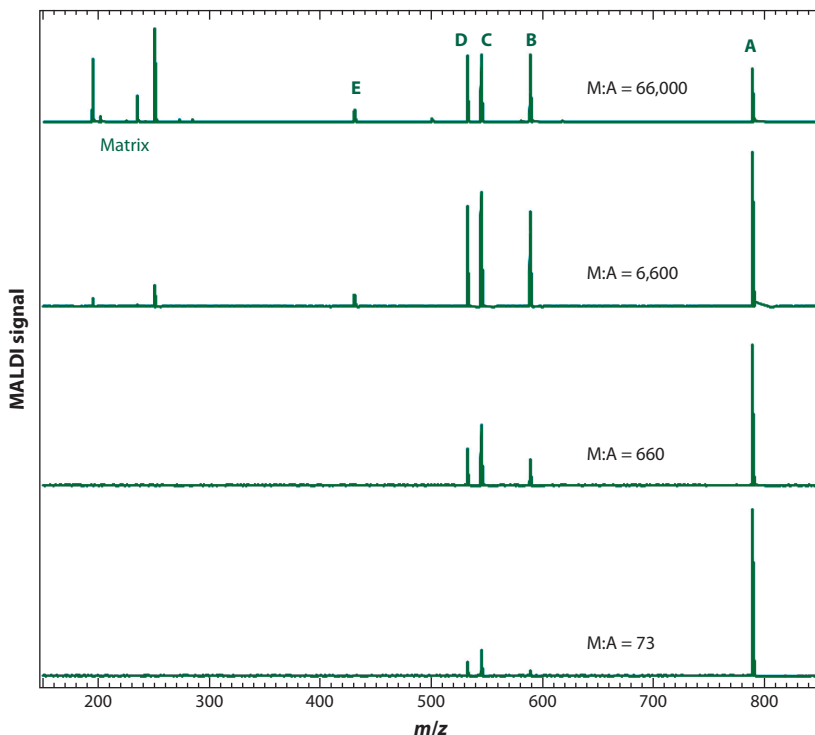


Figure 7

The analyte suppression effect in an equimolar mix of five analytes in DCTB matrix. All analytes are observed as radical cations; secondary reactions involve electron transfer. Analytes with low ionization potential (IP) values suppress those with higher IP values. The IP values for analytes A–E are 6.04, 6.28, 6.45, 6.50, and 7.06 eV, respectively. The IP of the DCTB matrix is approximately 8.2 eV. See also Reference 30. Abbreviations: DCTB, *trans*-2-[3-(4-*tert*-butylphenyl)-2-methyl-2-propenylidene]malononitrile; M:A, matrix:analyte molar ratio; MALDI, matrix-assisted laser desorption/ionization.

in **Figure 7** are an example. The IP value of analyte D (6.50 eV) is higher than that of analyte C (6.45 eV), but analyte C is suppressed slightly more than analyte D. The effect in this case is not large; it plays a bigger role in the ratio of positive to negative ions, as discussed below.

Coupling of positive and negative ionization pathways. The importance of a full kinetic treatment of MALDI is demonstrated by studies of positive/negative analyte ion ratios (PNAIRs). Some peptides were measured in a series of matrices in both polarities. Even though the gas-phase basicities of the matrices, and hence the secondary reaction energetics, varied by 150 kJ/mol, the resulting PNAIR remained near unity (84, 85). CPCD calculations show that this is to be expected over relatively wide ranges of matrix–analyte secondary reaction energies (7, 86). Fast forward reactions form analyte ions at similar rates in both polarities. Reverse reactions have unfavorable ΔG values and are too slow to approach local equilibrium. PNAIRs remain near unity, unless reaction ΔG values and rates become very unequal in the two polarities.

If forward and reverse secondary reactions are not very different, the polarities are more strongly coupled, and the PNAIRs vary more. This has consequences for quantitation. Unless all analytes in a sample have sufficiently favorable secondary reaction energetics in both polarities, relative intensities will not reflect initial sample concentrations. It has been proposed, for example, that

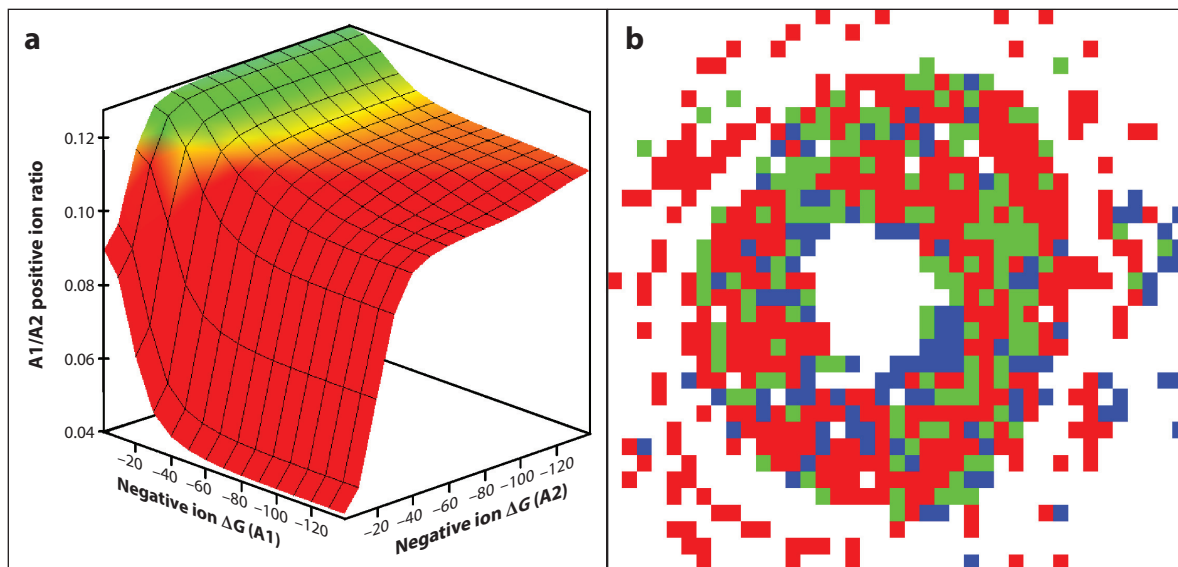


Figure 8

(a) CPCD predictions of MALDI analyte positive ion ratios as a function of negative ion secondary reaction energies, in kJ/mol. The positive-mode secondary reaction energies were taken to be identical for both analytes. (b) MALDI image of a dried drop spot of caffeine and yohimbine in a DHB matrix. Green pixels exhibited the correct 0.25 ion ratio of the preparation solution, within a factor of 2. In blue pixels, the caffeine signal was more than two times too high, and in red pixels, it was more than two times too low (less than 0.125). Red pixels dominate, comprising 61% of all usable pixels. See also Reference 82. Abbreviations: CPCD, coupled chemical and physical dynamics model; DHB, dihydroxybenzoic acid; MALDI, matrix-assisted laser desorption/ionization.

deprotonation reactions of many peptides with common matrices may be only weakly favorable (85), making quantitation of peptide mixtures more difficult in positive ion mode.

Figure 8 is an example of secondary reaction effects which are straightforwardly explained by the CPCD model. The measured analyte ion ratios are incorrect compared to the sample composition by more than a factor of 2 in 78% of the pixels. Of these, 61% are wrong in the same direction; the errors are not randomly distributed about the correct value. As shown in panel *a*, even if positive-mode energetics is equally favorable for both analytes, negative-mode energetics can determine whether the correct ion ratios are observed. Only a narrow range would give the expected result.

Quantitation with MALDI has long been regarded as problematic, and the CPCD helps to understand both why and when it is possible. The Kim group (87) proposed some techniques for better quantitation, as well as some rules for interpreting those methods in terms of a purely thermal equilibrium ionization model. Subsequently, Knochenmuss (88) showed that the techniques are fully consistent with the CPCD predictions and the effects discussed above. CPCD predictions were made for the ranges of parameters in which the rules will hold, many of which have been confirmed by MSE, ASE, and other studies. The Kim methods are effectively variants of spectral quality filters, selecting spectra within certain ranges of primary and secondary reaction extent.

Kinetic limitations in electron transfer ionization. For adduct ion transfer reactions, the CPCD secondary kinetics are nonlinearly but monotonically dependent on the reaction ΔG via the activation energies. As noted above, ET may slow at large negative ΔG values. Forward

secondary reactions may be affected, but ion recombination is the most energetically favorable reaction in MALDI. Marcus ET rate inversion therefore reduces ion losses more than it modulates ion formation (48). Evidence for this was found in MALDI analysis of ionic liquids, in that the liquids with the highest binding energy gave the strongest signals (49, 89).

CONCLUSIONS

The CPCD model includes primary ionization, secondary ion-molecule reactions and coupling of these processes to the spatially inhomogeneous and dynamic ablation event. It was initially developed for the 2,5-DHB matrix, in which primary ionization by singlet pooling occurs. It has been successfully extended to eight matrices, including some with strong intersystem crossing and probable triplet pooling. It has also been extended to matrix-substrate electronic coupling and confined ablation. The CPCD model exists in two forms depending on whether a microscopic picture is needed or local averaging is sufficient. It has encompassed PT, cation adduction, and ET.

Data of many types have been compared with CPCD predictions over many years. The CPCD model has proved consistent, qualitatively and often quantitatively, with the data. Many of the data are not consistent with alternate models, particularly those invoking thermal equilibrium. The CPCD is a framework that is expected to continue to evolve as information emerges on MALDI phenomena and matrix properties. Perhaps most importantly, the CPCD model has provided a means for rationally planning and interpreting MALDI data, making it relevant for analysts in their daily work.

DISCLOSURE STATEMENT

The author is not aware of any affiliations, memberships, funding, or financial holdings that might be perceived as affecting the objectivity of this review.

LITERATURE CITED

1. Karas M, Bachmann D, Hillenkamp F. 1985. Influence of the wavelength in high-irradiance ultraviolet laser desorption mass spectrometry of organic molecules. *Anal. Chem.* 57:2935–39
2. Karas M, Bachmann D, Bahr U, Hillenkamp F. 1987. Matrix-assisted ultraviolet laser desorption of non-volatile compounds. *Int. J. Mass Spectrom. Ion Proc.* 78:53–68
3. Dreisewerd K. 2003. The desorption process in MALDI. *Chem. Rev.* 103:395–426
4. Knochenmuss R. 2006. Ion formation mechanisms in UV-MALDI. *Analyst* 131:966–86
5. Knochenmuss R. 2002. A quantitative model of ultraviolet matrix-assisted laser desorption and ionization. *J. Mass Spectrom.* 37:867–77
6. Knochenmuss R. 2003. A quantitative model of UV-MALDI including analyte ion generation. *Anal. Chem.* 75:2199
7. Knochenmuss R. 2009. A bipolar rate equation model of MALDI primary and secondary ionization processes, with application to positive/negative analyte ion ratios and suppression effects. *Int. J. Mass Spectrom.* 285:105–13
8. Niu S, Zhang W, Chait BT. 1998. Direct comparison of infrared and ultraviolet wavelength matrix-assisted laser desorption/ionization mass spectrometry of proteins. *J. Am. Soc. Mass Spectrom.* 9:1–7
9. Chen X, Carroll JA, Beavis RC. 1998. Near-ultraviolet-induced matrix-assisted laser desorption/ionization as a function of wavelength. *J. Am. Soc. Mass Spectrom.* 9:885–91
10. Lu I-C, Lee CH, Lee Y-T, Ni C-K. 2015. Ionization mechanism of matrix-assisted laser desorption/ionization. *Annu. Rev. Anal. Chem.* 8:21–39
11. Bae YJ, Kim MS. 2015. A thermal mechanism of ion formation in MALDI. *Annu. Rev. Anal. Chem.* 8:41–60

12. Karas M, Glückmann M, Schäfer J. 2000. Ionization in matrix-assisted laser desorption ionization: Singly charged molecular ions are the lucky survivors. *J. Mass Spectrom.* 35:1–12
13. Jaskolla TW, Karas M. 2011. Compelling evidence for Lucky Survivor and gas phase protonation: the unified MALDI analyte protonation mechanism. *J. Am. Soc. Mass Spectrom.* 22:976–88
14. Karas M, Krueger R. 2003. Ion formation in MALDI: the cluster ionization mechanism. *Chem. Rev.* 103:427–39
15. Ehring H, Sundqvist BUR. 1995. Studies of the MALDI process by luminescence spectroscopy. *J. Mass Spectrom.* 30:1303–10
16. Ehring H, Sundqvist BUR. 1996. Excited-state relaxation processes of MALDI-matrices studied by luminescence spectroscopy. *Appl. Surf. Sci.* 96:577–80
17. Lüdemann H-C, Redmond RW, Hillenkamp F. 2002. Singlet-singlet annihilation in ultraviolet MALDI studied by fluorescence spectroscopy. *Rapid Commun. Mass Spectrom.* 16:1287–94
18. Setz P, Knochenmuss R. 2005. Exciton mobility and trapping in a UV-MALDI matrix. *J. Phys. Chem. A* 109:4030–37
19. Ehring H, Karas M, Hillenkamp F. 1992. Role of photoionization and photochemistry in ionization processes of organic molecules and relevance for matrix-assisted laser desorption/ionization mass spectrometry. *Org. Mass Spectrom.* 27:427–80
20. Liao P-C, Allison J. 1995. Ionization processes in matrix-assisted laser desorption/ionization mass spectrometry: matrix-dependent formation of $[M+H]^+$ versus $[M+Na]^+$ ions of small peptides and some mechanistic comments. *J. Mass Spectrom.* 30:408–23
21. Karbach V, Knochenmuss R. 1998. Do single matrix molecules generate primary ions in ultraviolet matrix-assisted laser desorption/ionization? *Rapid Commun. Mass Spectrom.* 12:968–74
22. Lin Q, Knochenmuss R. 2001. Two-photon ionization thresholds of matrix-assisted laser desorption/ionization matrix clusters. *Rapid Commun. Mass Spectrom.* 15:1422–26
23. Demirev P, Westman A, Reimann CT, Håkansson P, Barofsky D, et al. 1992. Matrix-assisted laser desorption with ultra-short laser pulses. *Rapid Commun. Mass Spectrom.* 6:187–91
24. Riahi K, Bolbach G, Brunot A, Breton F, Spiro M, Blais J-C. 1994. Influence of laser focusing in matrix-assisted laser desorption/ionization. *Rapid Commun. Mass Spectrom.* 8:242–47
25. Beavis RC. 1992. Phenomenological models for matrix-assisted laser desorption ion yields near the threshold fluence. *Org. Mass Spectrom.* 27:864–68
26. Soltwisch J, Jaskolla TW, Hillenkamp F, Karas M, Dreisewerd K. 2012. Ion yields in UV-MALDI mass spectrometry as a function of excitation laser wavelength and optical and physico-chemical properties of classical and halogen-substituted MALDI matrixes. *Anal. Chem.* 84:6567–76
27. Asfandiarov NL, Pshenichnyuk SA, Fokin AI, Lukin VG, Fal'ko VS. 2002. Electron capture negative ion mass spectra of some typical MALDI matrices. *Rapid Commun. Mass Spectrom.* 16:1760–65
28. Pshenichnyuk SA, Asfandiarov NL. 2004. The role of free electrons in MALDI: electron capture by molecules of α -cyano-4-hydroxycinnamic acid. *Eur. J. Mass Spectrom.* 10:477–86
29. Zenobi R, Knochenmuss R. 1998. Ion formation in MALDI mass spectrometry. *Mass Spectrom. Rev.* 17:337
30. Hoteling AJ, Nichols WF, Giesen DJ, Lenhard JR, Knochenmuss R. 2006. Electron transfer reactions in LDI and MALDI: factors influencing matrix and analyte ion intensities. *Eur. J. Mass Spectrom.* 12:345–58
31. Liu B-L, Charkin OP, Klemenko N, Chen CW, Wang Y-S. 2010. Initial ionization reaction in matrix-assisted laser desorption/ionization. *J. Phys. Chem. B* 114:10853–59
32. Knochenmuss R. 2014. Energetics and kinetics of thermal ionization models of MALDI. *J. Am. Soc. Mass Spectrom.* 25:1521–27
33. Lippa TP, Eustis SN, Wang D, Bowen KH. 2007. Electrophilic properties of common MALDI matrix molecules. *Int. J. Mass Spectrom.* 268:1–7
34. El-Sayed MA. 1968. The triplet state: its radiative and nonradiative properties. *Acc. Chem. Res.* 1:8–16
35. Jacques P, Allonas X, Sarbach A, Haselbach E, Vauthey E. 2003. Tuning the ion formation process from triplet-triplet annihilation to triplet-mediated photoionization. *Chem. Phys. Lett.* 378:185–91
36. Hoyer T, Tuszynski W, Lienau C. 2007. Ultrafast photodimerization dynamics in α -cyano-4-hydroxycinnamic and sinapinic acid crystals. *Chem. Phys. Lett.* 443:107–12

37. Hoyer T. 2009. *Stationäre und zeitaufgelöste Photolumineszenz-Spektroskopie zur Analyse ultraschneller Photoreaktionen in MALDI- und Solarzellenproben*. PhD Thesis, Carl von Ossietzky Universität Oldenburg, Oldenburg, Ger.
38. Hoyer T, Tuszynski W, Lienau C. 2010. Competing ultrafast photoinduced quenching reactions in cinnamic acid peptide blends. *Phys. Chem. Chem. Phys.* 12:13052
39. Knochenmuss R. 2014. MALDI mechanisms: wavelength and matrix dependence of the coupled photo-physical and chemical dynamics model. *Analyst* 139:147–56
40. Miller DR. 1988. Free jet sources. *Atomic Mol. Beam Methods* 1:14–43
41. Knochenmuss R, Zhigilei LV. 2005. A molecular dynamics model of UV-MALDI including ionization processes. *J. Phys. Chem. B* 109:22947–57
42. Handschuh M, Nettesheim S, Zenobi R. 1998. Laser-induced molecular desorption and particle ejection from organic films. *Appl. Surf. Sci.* 137:125–35
43. Zhigilei LV, Kodali PBS, Garrison BJ. 1997. Molecular dynamics model for laser ablation and desorption of organic solids. *J. Phys. Chem. B* 101:2028–37
44. Kinsel G, Knochenmuss R, Setz P, Land CM, Goh S-K, et al. 2002. Ionization energy reductions in small 2,5-dihydroxybenzoic acid-proline clusters. *J. Mass Spectrom.* 37:1131–40
45. Yassin FH, Marynick DS. 2006. Computational study of matrix-peptide interactions in MALDI mass spectrometry: interactions of 2,5- and 3,5-dihydroxybenzoic acid with the tripeptide valine-proline-leucine. *J. Phys. Chem. A* 110:3820–25
46. Knochenmuss R. 2004. Photoionization pathways and free electrons in UV-MALDI. *Anal. Chem.* 76:3179–84
47. Agmon N. 1981. From energy profiles to structure–reactivity correlations. *Int. J. Chem. Kinet.* 13:333–65
48. Knochenmuss R, Zhigilei LV. 2012. What determines MALDI ion yields? A molecular dynamics study of ion loss mechanisms. *Anal. Bioanal. Chem.* 402:2511–19
49. Knochenmuss R. 2013. MALDI and related methods: a solved problem or still a mystery? *Mass Spectrom. (Jpn.)* 2:S0006
50. Jaskolla TW, Karas M. 2008. Using fluorescence dyes as a tool for analyzing the MALDI process. *J. Am. Soc. Mass Spectrom.* 19:1054–61
51. Kirmess KM, Knochenmuss R, Blanchard GJ, Kinsel GR. 2016. MALDI ionization mechanisms investigated by comparison of isomers of dihydroxybenzoic acid. *J. Mass Spectrom.* 51:79–85
52. Knochenmuss R, Vertes A. 2000. Time-delayed 2-pulse studies of MALDI matrix ionization mechanisms. *J. Phys. Chem. B* 104:5406–10
53. Bae YJ, Shin YS, Moon JH, Kim MS. 2012. Degree of ionization in MALDI of peptides: thermal explanation for the gas-phase ion formation. *J. Am. Soc. Mass Spectrom.* 23:1326–35
54. Tsai M-T, Lee S, Lu I-C, Chu KY, Liang C-W, et al. 2013. Ion-to-neutral ratio of 2,5-dihydroxybenzoic acid in matrix-assisted laser desorption/ionization. *Rapid Comm. Mass Spectrom.* 27:955–63
55. Lu I-C, Chu KY, Lin C-Y, Wu S-Y, Dyakov YA, et al. 2015. Ion-to-neutral ratios and thermal proton transfer in matrix-assisted laser desorption/ionization. *J. Am. Soc. Mass Spectrom.* 26:1242–51
56. Knochenmuss R. 2015. Ion yields in the coupled chemical and physical dynamics model of MALDI. *J. Am. Soc. Mass Spectrom.* 26:1645–48
57. Horneffer V, Forsmann A, Strupat K, Hillenkamp F, Kubitscheck U. 2001. Localization of analyte molecules in MALDI preparations by confocal laser scanning microscopy. *Anal. Chem.* 73:1016–22
58. Salum ML, Itovich LM, Erra-Balsells R. 2013. Z-sinapinic acid: the change of the stereochemistry of cinnamic acids as rational synthesis of a new matrix for carbohydrate MALDI-MS analysis. *J. Mass Spectrom.* 48:1160–69
59. Kirmess KM, Knochenmuss R, Blanchard GJ. 2014. Excited state dynamics in the MALDI matrix 2,4,6-trihydroxyacetophenone: evidence for triplet pooling charge separation reactions. *Rapid Commun. Mass Spectrom.* 28:2134–40
60. Land CM, Kinsel GR. 1998. Investigation of the mechanism of intracluster proton transfer from sinapinic acid to biomolecular analytes. *J. Am. Soc. Mass Spectrom.* 9:1060–67
61. Land CM, Kinsel GR. 2001. The mechanism of matrix to analyte proton transfer in clusters of 2,5-dihydroxybenzoic acid and the tripeptide VPL. *J. Am. Soc. Mass Spectrom.* 12:726–31

62. Kinsel GR, Zhao Q, Narayanasamy J, Yassin F, Rasika Dias HV, et al. 2004. Arginine/2,5-dihydroxybenzoic acid clusters: an experimental and theoretical study of the gas-phase and solid-state systems. *J. Phys. Chem. A* 108:3153–61
63. McCombie G, Knochenmuss R. 2006. Enhanced MALDI ionization efficiency at the metal-matrix interface: practical and mechanistic consequences of sample thickness and preparation method. *J. Am. Soc. Mass Spectrom.* 17:737–45
64. Knochenmuss R, McCombie G, Faderl M. 2006. The dependence of MALDI ion yield on metal substrates: photoelectrons from the metal versus surface-enhanced matrix photoionization. *J. Phys. Chem. A* 110:12728–33
65. Knochenmuss R, Zhigilei LV. 2010. Molecular dynamics simulations of MALDI: laser fluence and pulse width dependence of plume characteristics and consequences for matrix and analyte ionization. *J. Mass Spectrom.* 45:333–46
66. Fournier I, Brunot A, Tabet J-C, Bolbach G. 2002. Delayed extraction experiments using a repulsive potential before ion extraction: evidence of clusters as ion precursors in UV-MALDI. Part I: dynamical effects with the matrix 2,5-dihydroxybenzoic acid. *Int. J. Mass Spectrom.* 213:203–15
67. Fournier I, Brunot A, Tabet J-C, Bolbach G. 2005. Delayed extraction experiments using a repulsive potential before ion extraction: evidence of non-covalent clusters as ion precursors in UV MALDI. Part II: dynamic effects with alpha-cyano-4-hydroxycinnamic acid matrix. *J. Mass Spectrom.* 40:50–59
68. Alves S, Fournier I, Afonso C, Wind F, Tabet J-C. 2006. Gas-phase ionization/desolvation processes and their effect on protein charge state distributions under MALDI conditions. *Eur. J. Mass Spectrom.* 12:369–83
69. Bökelmann V, Spengler B, Kaufmann R. 1995. Dynamical parameters of ion ejection and ion formation in matrix-assisted laser desorption/ionization. *Eur. Mass Spectrom.* 1:81–93
70. Dreisewerd K, Schürenberg M, Karas M, Hillenkamp F. 1995. Influence of the laser intensity and spot size on the desorption of molecules and ions in matrix-assisted laser-desorption/ionization with a uniform beam profile. *Int. J. Mass Spectrom. Ion Proc.* 141:127–48
71. Feldhaus D, Menzel C, Berkenkamp S, Hillenkamp F. 2000. Influence of the laser fluence in infrared matrix-assisted laser desorption/ionization with a 2.94 μm Er:YAG laser and a flat-top beam profile. *J. Mass Spectrom.* 35:1320–28
72. Guenther S, Koestler M, Schulz O, Spengler B. 2010. Laser spot size and laser power dependence of ion formation in high resolution MALDI imaging. *Int. J. Mass Spectrom.* 294:7–15
73. Qiao H, Spicer V, Ens W. 2008. The effect of laser profile, fluence and spot size on sensitivity in orthogonal-injection MALDI mass spectrometry. *Rapid Commun. Mass Spectrom.* 22:2779–90
74. Schuerenberg M, Dreisewerd K, Kamanabrou S, Hillenkamp F. 1998. Influence of the sample temperature on the desorption of matrix molecules and ions in MALDI. *Int. J. Mass Spectrom.* 172:89
75. Wallace WE, Arnould MA, Knochenmuss R. 2005. 2,5-Dihydroxybenzoic acid: laser desorption/ionization as a function of elevated temperature. *Int. J. Mass Spectrom.* 242:13–22
76. Walker BN, Razunguzwa T, Powell M, Knochenmuss R, Vertes A. 2009. Nanophotonic ion production from silicon microcolumn arrays. *Angew. Chem. Int. Ed.* 48:1669–72
77. Go EP, Apon JV, Luo G, Saghatelian A, Daniels RH, et al. 2005. Desorption/ionization on silicon nanowires. *Anal. Chem.* 77:1641–46
78. Luo GH, Chen Y, Daniels H, Dubrow R, Vertes A. 2006. Internal energy transfer in laser desorption/ionization from silicon nanowires. *J. Phys. Chem. B* 110:13381–86
79. Knochenmuss R. 2009. Laser desorption/ablation plumes from capillary-like restricted volumes. *Eur. J. Mass Spectrom.* 15:189–98
80. Knochenmuss R, Dubois F, Dale MJ, Zenobi R. 1996. The matrix suppression effect and ionization mechanisms in matrix-assisted laser desorption/ionization. *Rapid Commun. Mass Spectrom.* 10:871–77
81. Knochenmuss R, Karbach V, Wiesli U, Breuker K, Zenobi R. 1998. The matrix suppression effect in matrix-assisted laser desorption/ionization: application to negative ions and further characteristics. *Rapid Commun. Mass Spectrom.* 12:529–34
82. McCombie G, Knochenmuss R. 2005. Small-molecule MALDI using the matrix suppression effect to reduce or eliminate background interferences. *Anal. Chem.* 76:4990–97

83. Knochenmuss R, Stortelder A, Breuker K, Zenobi R. 2000. Secondary ion-molecule reactions in MALDI. *J. Mass Spectrom.* 35:1237–45
84. Dashtiev M, Wäfler E, Röhling U, Gorshkov M, Hillenkamp F, Zenobi R. 2007. Positive and negative analyte ion yield in matrix-assisted laser desorption/ionization. *Int. J. Mass Spectrom.* 268:122–30
85. Hillenkamp F, Wäfler E, Jecklin MC, Zenobi R. 2008. Positive and negative analyte ion yield in MALDI revisited. *Int. J. Mass Spectrom.* 285:114–19
86. Knochenmuss R. 2008. Positive/negative ion ratios and in-plume reaction equilibria in MALDI. *Int. J. Mass Spectrom.* 273:84–86
87. Ahn SH, Park KM, Bae YJ, Kim MS. 2013. Quantitative reproducibility of mass spectra in matrix-assisted laser desorption ionization and unraveling of the mechanism for gas-phase peptide ion formation. *J. Mass Spectrom.* 48:299–305
88. Knochenmuss R. 2013. MALDI ionization mechanisms: The coupled photophysical and chemical dynamics model correctly predicts “temperature”-selected spectra. *J. Mass Spectrom.* 48:998–1004
89. Moon JH, Shin YS, Bae YJ, Kim MS. 2011. Ion yields for some salts in MALDI: mechanism for the gas-phase ion formation from preformed ions. *J. Am. Soc. Mass Spectrom.* 23:162–70